18TH LISBON 2016
INTERNATIONAL SYMPOSIUM
ON APPLICATIONS OF LASER AND IMAGING TECHNIQUES TO FLUID MECHANICS
FROM 4 TO 7 OF JULY

PROCEEDINGS

OF THE

18th INTERNATIONAL

SYMPOSIUM ON

APPLICATION OF

LASER AND IMAGING

TECHNIQUES TO

FLUID MECHANICS

Towards high-resolution 3D flow field measurements at cubic meter scales

Daniel Schanz[1], Florian Huhn[1], Sebastian Gesemann[1], Uwe Dierksheide[2],
Remco van de Meerendonk[3], Peter Manovski[4], Andreas Schröder[1]

[1]German Aerospace Center (DLR), Institute of Aerodynamics and Flow Technology, Department of Experimental Methods, Göttingen, Germany; [daniel.schanz@dlr.de]

[2]LaVision GmbH, Anna-Vandenhoeck-Ring 19, Göttingen, Germany

[3]Aerospace Engineering Department, Delft University of Technology, 2629, The Netherlands

[4]Defence Science and Technology Organisation (DSTG), Australia

* Correspondent author: daniel.schanz@dlr.de

Keywords: Lagrangian Particle Tracking, LED volume illumination, Helium filled soap bubbles

ABSTRACT

We present results from two large-volume volumetric flow experiments. The first of these, investigating a thermal plume at low velocities (up to 0.35 m/s) demonstrates the abilities and requirements to reach volume sizes up to and probably beyond one cubic meter. It is shown that the use of Helium filled soap bubbles (HFSBs) as tracers, combined with pulsed LED illumination yields high particle image quality over large volume depths. A very uniform particle imaging, both in space as well as in time enables using high particle image concentrations (up to 0.1 ppp), while still being able to accurately reconstruct the flow using Shake-The-Box particle tracking.

The experiment consisted of time-resolved volumetric flow measurements of a convectional plume within a volume of approx. 0.55 m^3 (550 liters). The light yield needed for such a large scale measurement is realized by using HFSBs with 300 μm diameter as tracers and illuminating the measurement region using high-power, scalable arrays of white LEDs. Applying the Shake-The-Box algorithm, up to 275,000 bubbles could be tracked simultaneously. Interpolating the results on a regular grid (using 'FlowFit') reveals a multitude of flow structures. The setup can be scaled to larger volumes of several cubic meters, basically only being limited by the number and power of available LEDs and high-resolution cameras with sufficient frame-rate and pixel sizes.

A second experiment showcases the possibilities to reach higher flow velocities, while still measuring within a comparatively large volume, by applying high-speed imaging and advanced LED illumination. An impinging turbulent jet was investigated in volumes ranging from 13 to 47 liters, depending on the repetition rate of the camera system. The results show that even at a repetition rate of 3.9 kHz and flow speeds up to 17 m/s the tested system was able to deliver images that allowed for a reliable and accurate tracking of bubbles.

Again, the use of more LEDs would allow for larger volumes. New generations of high-speed cameras should enable the use of even higher flow speeds – thus enabling large-volume measurements in typical low speed wind tunnel experiments at high spatial resolution (provided enough HFSBs can be produced).

1. Introduction and Motivation

Time resolved volumetric flow measurements, using methods like TOMO PIV (Elsinga et al. 2006), 3D PTV (Maas et al. 1993, Malik et al. 1993) or Shake-The-Box (Schanz et al. 2016), are typically restricted to relatively small volume sizes in the order of <= 200 cm^3 (Scarano et al. 2015). This limitation stems from the small size of commonly used seeding material, in order to accurately follow the flow (~ 1 μm in air, 10 – 50 μm in water). Currently available high-repetition laser systems, which are typically used as light source, do not provide enough intensity to allow for illumination of larger volumes - even for the larger particles used in water experiments. However, seeding particles whose density approaches that of the medium can be of much larger size, while still accurately following the flow (Melling 1997). Following this thought, neutrally buoyant Helium filled soap bubbles (HFSB) have been used in air to allow for large scale flow measurements. Applications range from traceline-visualizations (Pounder 1956) over large-scale 2D-PIV measurements (Müller et al. 2000, Bosbach et al. 2009) to three-dimensional tracking of single bubbles (Klimas 1973) and large-scale tomographic PIV of a convective flow (Kühn et al. 2011). Very recently, the feasibility of using HFSBs in wind tunnel facilities has been demonstrated (Scarano 2015).

While some the previous applications examined large measurement areas (Biwole et al. 2009, Klimas 1973), all of these were limited in particle number (e. g. tracing a few tens or hundreds of bubbles). The largest investigated volume that allowed the description of instantaneous flow structures was applied by Kühn et al (2011). A convection cell with a volume of approx. 56 liters was investigated using 2-pulse tomo-PIV. However, a large interrogation window size had to be chosen (48*48*24 mm), limiting the spatial resolution to large structures. The experiment reported by Scarano et al. (2015) was special in that it is the first application of HFBSs in a wind tunnel experiment. As Scarano et al. have shown, the production of enough bubbles to achieve a sufficient particle concentration within the measurement volume is a major topic for higher flow speeds. Due to the limitations in bubble number and due to the limits of the high-speed laser used for illumination, the volume size was restricted to 4.8 liters in this experiment and the interrogation windows were quite large (96x96x86 voxels).

The experiments discussed here avoid the problem of bubble production rate by operating in a closed chamber. LEDs provide a scalable light-source that is free of the typical artifacts of laser illumination (speckles, diffraction problems, etc.). HFSBs can be produced virtually mono-disperse and due to the light being reflected at the bubble surface (instead of scattered) uneven imaging between the different cameras is avoided. These features lead to a very high attainable image quality (as discussed in paragraph 2.4), which allows for a very reliable and accurate particle tracking using the Shake-The-Box (STB) algorithm. By applying a regularized interpolation scheme ('FlowFit', Gesemann et al. 2016) the locally highly accurate information is leveraged to maximize the spatial resolution (Schneiders et al. 2015).

2. Thermal plume investigation

2.1. Convection chamber

The experiments are performed in a cylindrical convection chamber with a height of 2.00 m and a diameter of 1.83 ,m (see Figure 1). Top and bottom plates are constructed of wood, the back wall is made of aluminum, and the transparent front window is acrylic glass of 1 mm thickness. Intransparent parts of the floor, walls and ceiling are painted black or covered with black adhesive film, in order to avoid scattered light and to improve the contrast of the particle images towards the background. The convection chamber is accessible from the back side through a door in the aluminum wall. The chamber is equipped with a circular perforated tube at the bottom to rinse it with pressurized air and remove seeding.

LED illumination enters through a plexiglas window of 1 m diameter in the ceiling, covered with a circular passe-partout (0.75 m diameter) that determines the width of the cylindrical measurement volume. The convective flow is forced by a standard 1500 W electric hotplate (188 mm diameter, Silva Homeline EKS 2121) that is placed a few centimeters below the measurement volume. It is covered by a black circular 250 mm diameter aluminum plate of 10 mm thickness that serves as a heat reservoir to keep the temperature constant over time.

Before conducting experiments, the hotplate is heated up for a few seconds to reach the desired temperature, and left some minutes until a uniform temperature distribution and a constant temperature is attained. Three temperature sensors are installed in the convection chamber to monitor the temperature of the heated aluminum plate, the air temperature 2 mm above the plate as a proxy for the maximum air temperature, and the ambient air temperature (see Figure 1 for positions of sensors). The accuracy of the absolute temperature measurement is estimated to be ±2°C, while the relative temperature differences, relevant for the convective flow, are accurate

within ±0.5°C. During the experiments, heat is provided by the aluminum plate, while the temperature was decreasing less than 0.5 K (see Figure 6).

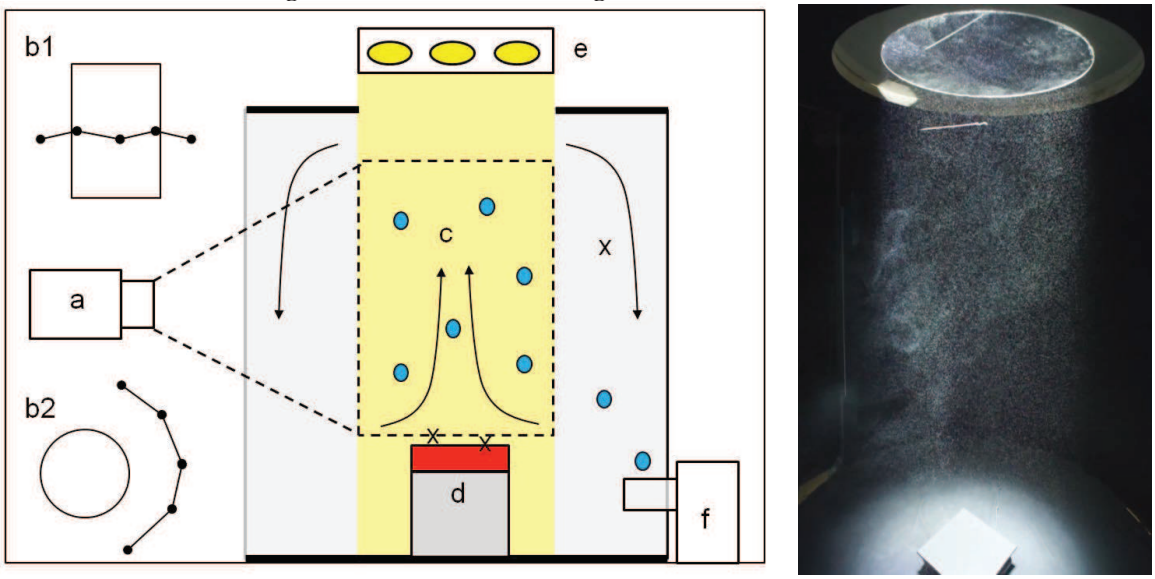

Figure 1: (left) Experimental setup of convection chamber: (a) cameras; (b1, b2) front and top view of camera configuration; (c) field of view (FOV), (d) hotplate; (e) LED array; (f) bubble generator; (x) positions of three temperature sensors

(right) Photograph of the interior of the convection chamber

2.2. Helium-filled soap bubbles

For PTV measurements, the flow is densely seeded with neutrally-buoyant helium-filled soap bubbles (HFSB) of 300µm diameter. They are produced by a bubble generator prototype of LaVision, based on the nozzle design presented by (Bosbach et al. 2009).

A nozzle consists of three concentric channels - providing helium, soap solution (ASAI 1035, Sage Action Inc.), and pressurized air, from the center outwards. It is covered by a cap with an orifice of 1.0 mm diameter.

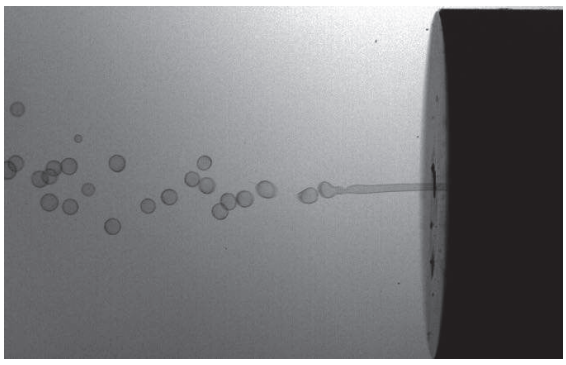

Figure 2: High-speed image (Exposure time 10μs, recording rate 1.5kHz) of the seeding nozzle

The two inner channels produce a thin helium-filled soap tube that is transported through the orifice by the surrounding air flow and breaks up into a single chain of equally sized bubbles in the increasingly turbulent air flow (see Figure 2).

Six nozzles are operated in parallel with a bubble production rate of ~ 45,000/s each, counted with a high speed camera directed to the outlet of the nozzle. The nozzles are directly placed at the bottom inside the convection chamber to enable a high seeding density in the large volume. HFSBs are injected vertically close to the wall to avoid the influence of the momentum of the nozzles' jet towards the center where the hotplate is located. Before an experiment, the chamber was seeded for 30 seconds to reach a high particle concentration. A waiting period of around 135 seconds follows to reach a homogeneous spatial distribution of the seeding and let decay the motion induced by the nozzles' jet.

We adjust neutral buoyancy of the HFSBs by varying the flow rate of helium such that a zero settling velocity is attained. Careful experiments by Scarano et al. (2015) show that HFSB follow the air flow at high accelerations of ~10^{1} m/s^{2} in a wind tunnel even for a variation of the helium flow rate by a factor of two. Since in our convective flow, accelerations are much smaller (g~10^{1} m/s, see results of STB), we expect the tracer to closely follow the air flow.

Soap bubbles burst, and the life time can be a limiting parameter especially for large convective flows that are typically slow and related to long time scales. Bosbach et al. (2009) estimate the life time of HFSB to be 1-2 min under similar conditions, e.g., room temperature and presumably relatively low relative air humidity in a lab.

2.3. LED light source

The measurement volume is illuminated by a LED array consisting of 7 standard collimated LED spotlights (Treble-Light, Power LED 20000) with an opening angle of 9° and 18,000 lm luminous flux at 170 W nominal electric power input each. One spotlight is composed of 48 LEDs with 3.5 W each. The LED array is located 1 m above the ceiling of the convection chamber and a passe-partout of 0.75 m diameter on the ceiling window defines the cylindrical measurement volume. In the experiment, the LED light source is synchronized with the camera system and is pulsed with a period of 3 ms at 29 Hz, corresponding to a 10 % duty cycle.

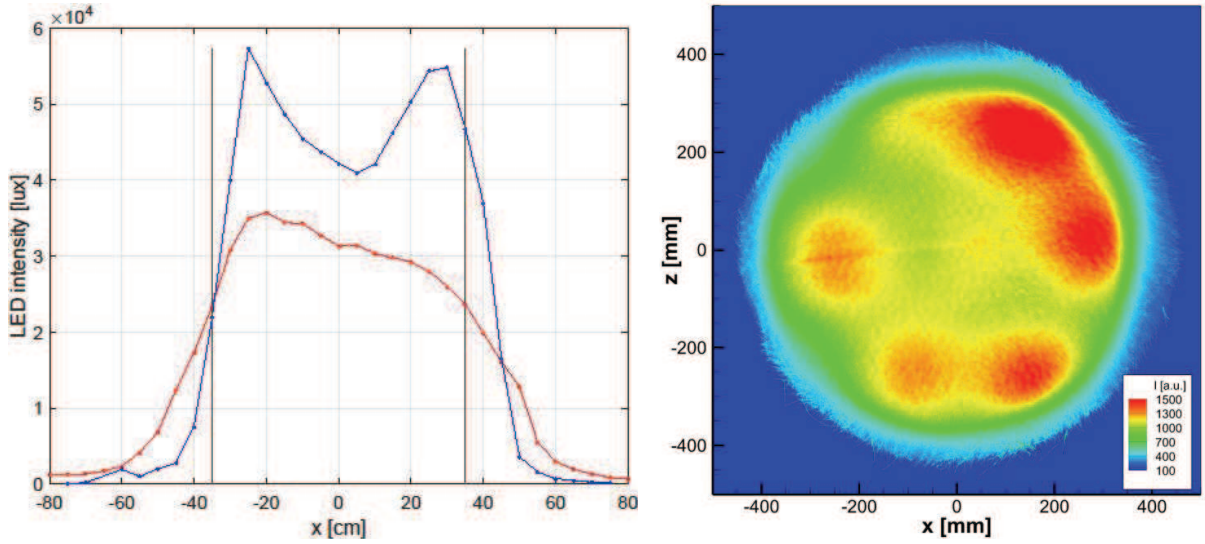

Figure 3: (Left) Intensity profile of continuous LED illumination across the measurement volume at a height of 110 cm (blue) and at the bottom of the convection cell (red) in the continuous mode. Black bars show the position of the passe-partout. (Right) Particle intensity as given by STB results, averaged over streamwise (y) direction

As a reference, we measure the horizontal profile of the continuous light intensity (light meter, Extech HD450) at the bottom of the convection chamber (red curve, Figure 3 left) and at a height of 1.10m across the measurement volume (blue curve). The illuminated volume is well defined by a sharp decay in light intensity, which helps to avoid light scattering from particles outside the measurement domain. An intensity dip in the center can be attributed to inhomogeneous distribution of LEDs in the light source and possible variations of intensity output between different LED arrays. Overall, the intensity of approximately 4.5 * 10^4 lux corresponds to ~ 17,000 lm over the whole area.

Another view on the light intensity distribution is given in Figure 3 (right), which depicts a 2D ensemble average of the intensity of all particles as identified by the STB tracking (see paragraph 3) over a run of 500 images. The x- and z- direction of the measurement volume were discretized in 2×2-pixel bins and all particles located within such a bin are averaged (thus averaging over the streamwise direction of space). The different intensity of the LED spots can be easily seen. The spot located at x= 200 mm, z= 200 mm appears to have nearly double the intensity of the weakest one, located at x= -200 mm, z= 200 mm. These findings document that great care should be taken before assembling the illumination arrays in order to achieve homogenous lighting conditions.

Additionally it can be seen that due to the opening angle of 9° the illuminated region is widened from 75 cm at the top window to around 80 cm in the measurement volume. Given the height of

approx. 110 cm, the total volume comprises approx. 550 liters.

2.4. Camera system

The camera setup consists of five cameras (pco.edge 5.5 sCMOS, PCO) with a resolution of 2560×2160 pixels. They are arranged in a flat M-configuration with a small height difference between neighboring cameras of 15 cm (see Figure 1 and Figure 4). The cameras are placed on a circle around the convection chamber with a distance of 2.25 m to the vertical center line of the cylindrical measurement volume such that the cameras look perpendicularly through the front window.

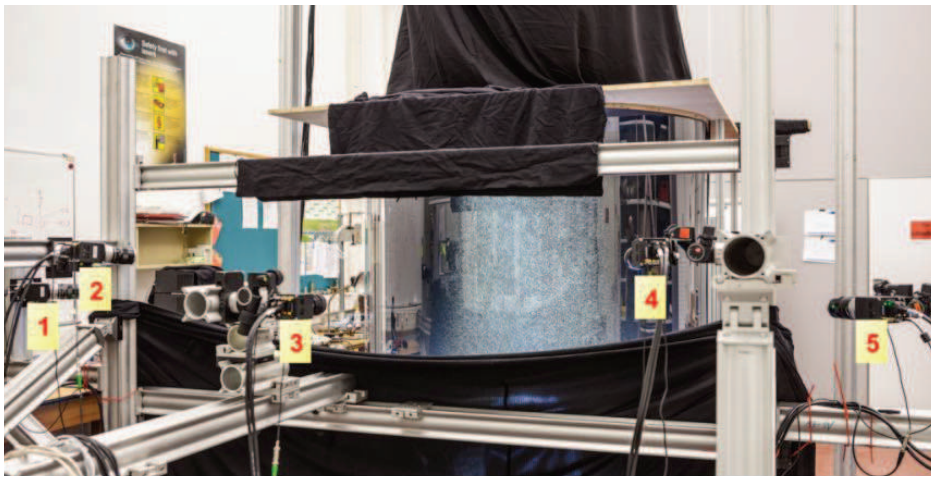

Figure 4: Photograph of the camera system and the convective cell.

The lines of sight of the outermost cameras have an angle >90° allowing for an accurate reconstruction of the particle position in all dimensions. The cameras are equipped with f=35mm lenses (Zeiss Contax) with the aperture set to $F_{\#} = 11$, yielding sufficient depth of field to image the volume with 0.8 m diameter. The cameras are rotated by 90°, so their FOV has a width of 0.85 m and a height of 1.1 m to capture the vertically extended cylindrical volume.

Figure 5: Unprocessed camera image (only background of 340 pixels subtracted, low seeding density, color

inverted). Sum of five consecutive images

The magnification is M = 0.016, corresponding to 0.4 mm/pix, so the observed velocities of up to 0.3 m/s result in a maximum particle shift of ~25 pix between two images. With this magnification, the maxima of the two glare points - reflections at two points of the bubble (Kühn et al. 2011, Scarano et al. 2015) - fall into one pixel, such that we obtain an isotropic circular particle image with a single peak. The image quality in general is very high. The production of the bubbles is a very stable process, leading to a monodisperse distribution of particle sizes at around 300 µm. Additionally, the absence of coherent light prevents effects of interferences or speckles. An example of the high image quality is given in Figure 5, showing a detail of a sample run at low seeding density and random flow. The sum of five consecutive images is shown, documenting the uniformity in particle imaging - both between the different bubbles, as well as in time for a single bubble.

For the 3D calibration of the cameras, a planar calibration target is set into the convection chamber and shifted to three positions, each 200 mm apart. Image acquisition, synchronization of cameras and the light source were controlled through the DaVis software (LaVision). The accuracy of the volumetric calibration was enhanced using Volume-Self-Calibration (Wieneke 2007); the particle imaging was calibrated, yielding a volumetrically resolved Optical Transfer Function (OTF, Schanz et al. 2013a).

All five cameras were connected to a single PC and the data was recorded directly to hard disc. The recording frequency of 29 Hz reflects the maximum write rate that was attainable. Connecting each camera to a single PC would allow for a repetition rate up to 100 Hz.

3. Data evaluation

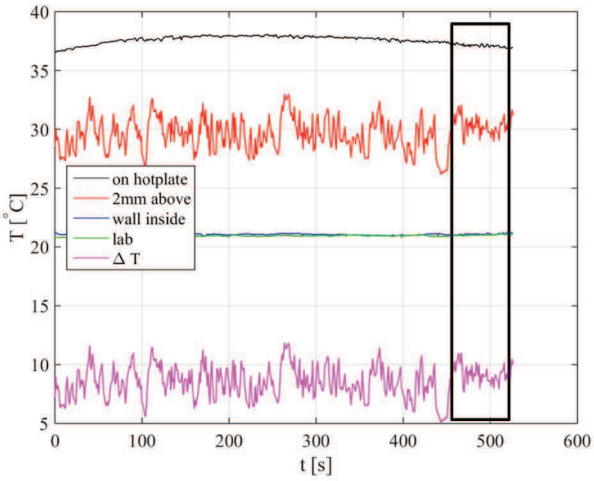

Figure 6: Temperature log for the different sensors, including a relaxation time. Measurement time (1000

images) marked by rectangle

For this feasibility study a single measurement run was chosen from the available material, which features suitable conditions (high particle density, large particle shift) to assess how well the STB-evaluation copes with the current setup. The seeding density was found to be approx. 0.08 ppp in the center of the image (see Figure 7, left). The temperature difference between the air directly over the hot plate and the surrounding air was approximately 8°C (see Figure 6), which led to maximum velocities of around 0.35 m/s, corresponding to a maximum particle shift of nearly 30 pixels. 1000 images were recorded at a frequency of 29 Hz, of which 500 were evaluated using STB. Image preprocessing consisted of subtracting the smoothed minimum image and a constant of 50 counts.

3.1. Shake-The-Box processing

The DLR in-house STB algorithm was applied. For details of the method, please refer to (Schanz et al. 2016). The following parameters were applied to the current dataset: The number of triangulation iterations was set to 2 - using an allowed triangulation error of 1.0 pixel - followed by one triangulation iteration using a reduced set of cameras. Each of these was followed by five shake-iterations (n_1= 2, n_2=1, m = 5, ε = 1.0; see (Wieneke 2013)). For the initialization phase (the first four images), the number of triangulations was doubled. No help of a predictor in form of a vector field gained by TOMO-PIV processing was used in this case. As shown in Figure 8 (left), the number of tracked particles quickly increases with the number of processed images. After the initialization phase, around 53,000 tracks of length four are found. This number rises to 110,000 only three time-steps later and reaches 200,000 at time-step 18. For this first pass (going forward in time), the number of tracked particles saturates at just over 250,000 after about 80 images. From there on, the tracked particle number decreases, as bubbles burst and disappear from the tracking system. When reaching the end of the time-series, time is reversed and the algorithm walks backwards in time through the dataset. By doing so, known tracks that were not

immediately found within the first pass are extended and the first time-steps, where the tracking system was not yet converged in the first pass, are completely reconstructed.

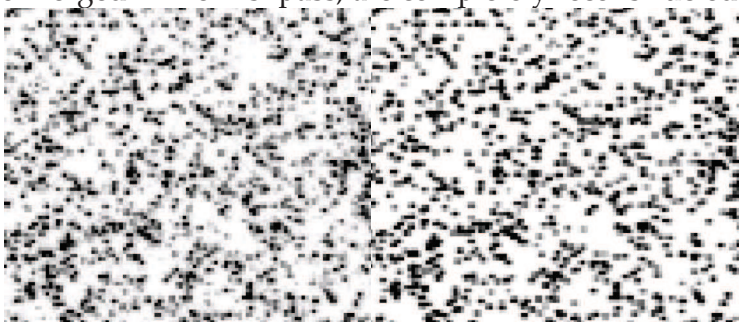

Figure 7: (Left) detail from camera image; (right) reprojection of particle distribution as reconstructed by STB.

At maximum, around 275,000 particles are simultaneously tracked in the second pass. To the knowledge of the authors, this is an unprecedented number for particle tracking methods, which typically operate with hundreds or a few thousand particles within the same image.

Figure 7 compares the camera image to the virtual image, created by reprojecting all tracked particles. The high quality of the tracking process is documented in Figure 8 (right), which shows a statistic of the track length after pass 2. A very distinct peak can be seen at 500 images, showing that over 81,000 particles have been tracked over the whole time-series. These are particles slowly moving in the entrainment region. The rest of the tracks show lengths that are quite evenly distributed, reflecting the fact that many particles are transported at different speeds out of the volume. The computational effort, combined for both passes, is around 220 seconds per time-step. For comparison, the volume corresponds to a voxel space of 1960×2696×1960 voxels when using a voxel-to-pixel ratio of 1.0. Reconstruction and correlation times of such spaces of 10 teravoxel are very high.

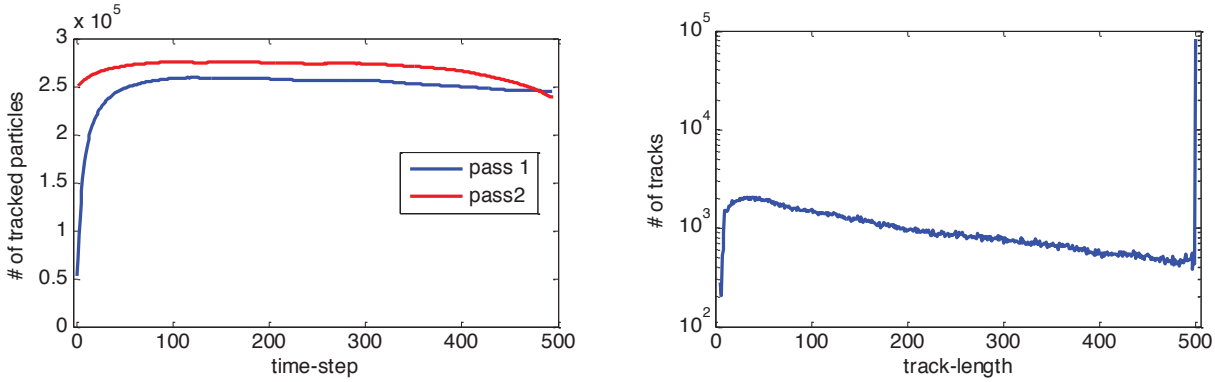

Figure 8: (Left) Development of number of tracked particles over time for both passes of STB; (right) track-length statistics after pass 2.

Following the second pass, the particle tracks are temporally filtered by means of an optimal Wiener filter, being represented by a series of 1D-B-Splines. On average, the particles are moved 0.116 px from their original position (0.046 px in x-, 0.040 px in y- and 0.083 px in z-direction) by the fit procedure. The velocity- and acceleration values are calculated as derivatives of the polynomial.

4. Flow field results

Figure 9 shows an instantaneous flow situation, depicted by ca. 275,000 tracks, whose velocity vectors are drawn for three consecutive time-steps and color-coded by streamwise velocity. Views from the front side and the top are provided. A large region of slowly moving particles, surrounding the thermal plume can be seen. The maximum velocity values are approx. 0.35 m/s, corresponding to a particle shift of nearly 30 pixels. The central regions can be better recognized in Figure 10, which shows the same tracks as Figure 9, albeit only a middle slice of 10 cm depth is shown, both for the x/y- and the z/y-plane. In general, the shape of the plume was varying in time quite visibly; in this time instant it can be seen that the plume is broadened in the z-direction, compared to the x-direction.

Vortical structures can already be identified by looking at the particle tracks; however a quantitative description is possible when quantities like vorticity or the Q-criterion are available. To this end, the discrete Lagrangian velocity- and acceleration information at the particle location is interpolated onto an Eulerian grid using the DLR in-house algorithm 'FlowFit' (Gesemann et al. 2016).

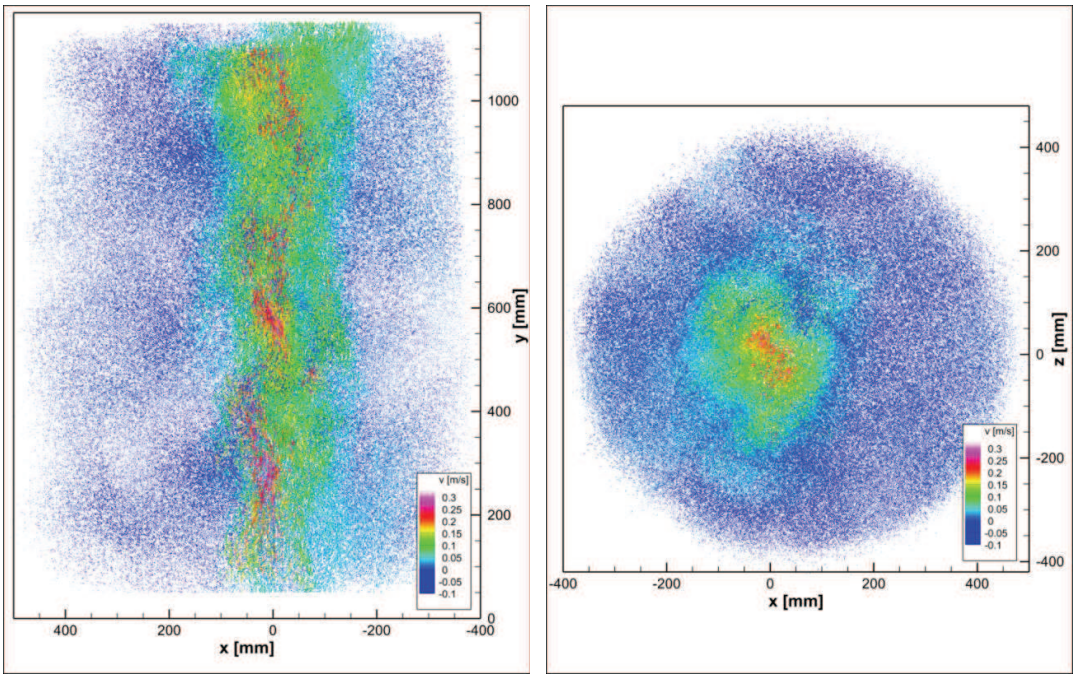

Figure 9: Front- and top view of the measurement volume, showing approx. 275.000 tracks for three consecutive time-steps, connected by the velocity vectors. Color-coding by streamwise velocity (v).

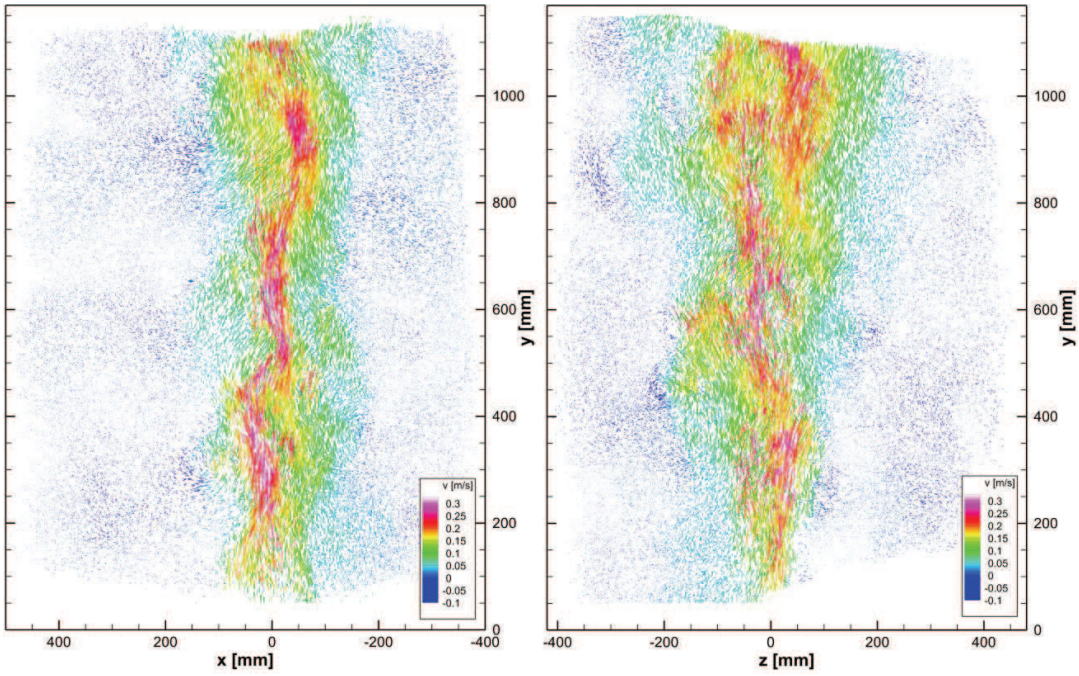

Figure 10 Front- and side view of the measurement volume, showing a middle slice of 100 mm thickness. Tracks shown for three consecutive time-steps, connected by the velocity vectors; color-coding by streamwise velocity (v).

The method models each component of the flow field as a weighted sum of three-dimensional and evenly spaced cubic B-splines. In order to evaluate this flow field on arbitrary coordinates, the weights have to be determined according to the known flow speeds at certain locations (being the particles with their velocity and acceleration). This results in a linear equation system where for each known flow speed at some particular position three equations are created. In addition to these equations based on the measurements other equations are used to regularize the equation system by penalizing non-zero curvatures (which is known in combination with spline fitting as "smoothing spline") and optionally (when the flow can be regarded as incompressible) by penalizing non-zero divergencies on a regular grid. This results in an overdetermined system where measurements and different kinds of regularizations can be weighted differently depending on how strong the smoothing effect should be, for example. This equation system is solved iteratively via the conjugate-gradient algorithm. The resulting flow field is then sampled on a regular grid including its spatial derivatives so that the derived values, such as vorticity or Q-criterion can be computed without numerical differentiation (Gesemann et al. 2016). For results of STB+FlowFit applied on Case D of the fourth international PIV Challenge, please see the DLR results in Kähler et al. (2016).

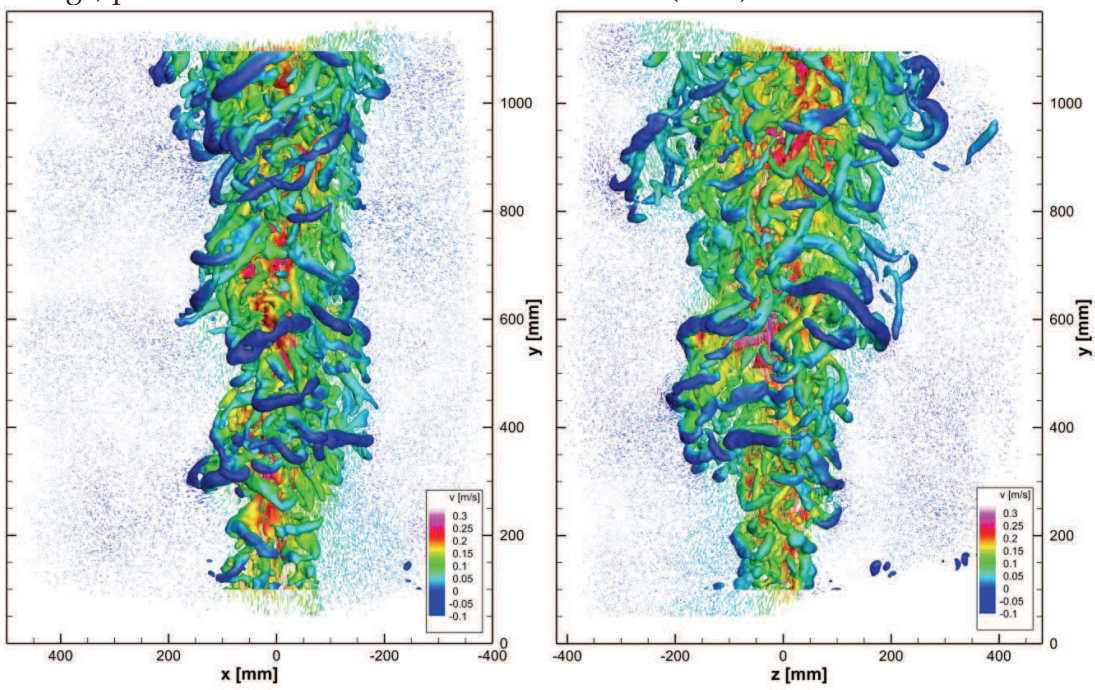

Figure 11: Isosurfaces of Q-criterion for one time-instant, color-coded by streamwise velocity. (Left) front view (looking from the cameras); (right) side view. Isosurfaces superimposed on the tracks as shown in Figure 10

FlowFit was applied to each of the 500 time-steps, taking velocities of the respective tracked

particles as data base. The B-spline system is setup, such that on average ten B-spline cells are present for every particle (0.1 *particles per cell*), leading to a spacing of approx. 8 mm between the cells. The compressibility constraint was applied (which is reasonable in the first approximation, given the low velocities and temperature gradients present), such that a penalization was put on divergency. 1500 iterations of the conjugate-gradient algorithm are applied to solve the equation system. The resulting continuous function is closely sampled on a grid with 3 mm spacing, ultimately leading to vector volumes of 266×333×266 vectors.

An example of the results gained by applying FlowFit to the STB track data is given in Figure 11, which shows isosurfaces of Q-criterion for the middle of the three time-steps shown in Figure 9 and Figure 10. The full amount and extent of the thermal flow structures becomes apparent. Long, undisturbed vortices are identified in the shear layers surrounding the center of the plume, while the central structures are smaller, but show equal strength. When looking at a time-series of such images a high temporal coherence is noticeable. The high quality of the tracking process translates directly into the quality of the Eulerian representation.

The high position accuracy, which is achievable due to the image quality, allows for an evaluation of particle acceleration (material derivative) - being the second derivative of space. Figure 12 shows tracks for the same time-steps as discussed before, color-coded by streamwise acceleration. Especially the detail view reveals that the acceleration and deceleration of particles drawn into flow structures is rendered smoothly by the tracking scheme. Just as for velocity, the acceleration can be interpolated onto an Eulerian grid using FlowFit. Figure 12 (right) displays the result of applying FlowFit to the particle accleration distribution in Figure 12 (left), with a penalization of rotation (therefore implying that viscosity effects plays a minor rule, which should hold for the small temperature differences present). Isosurfaces of streamwise acceleration indicate the regions of acceleration and deceleration above and below vortices (compare to Figure 11, right).

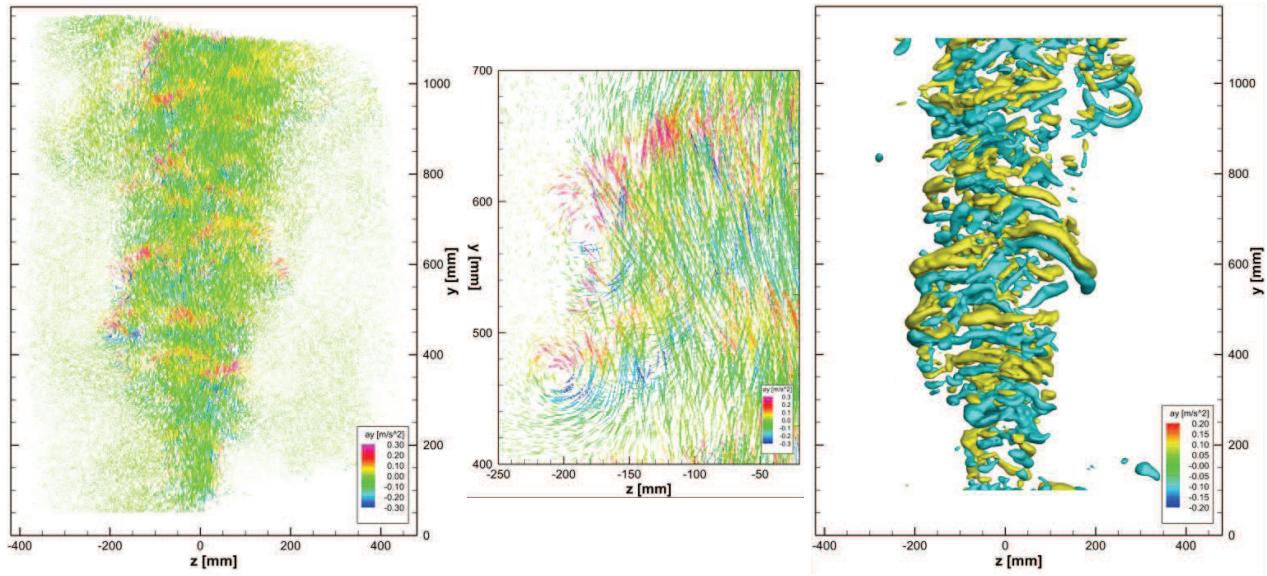

Figure 12: (Left) Tracks for three consecutive time-steps, color-coded by streamwise acceleration. Volume reduced to a middle slice of 200 mm; (Middle): Detail view from (left); (rigth) Isosurfaces of streamwise acceleration as extracted by FlowFit.

5. High-repetition measurement on an Impinging Jet

The results of the previous chapters demonstrate that combining HFSBs as tracer particles with LED illumination allows for a very accurate particle tracking in large volumes. In order to overcome the limitations in flow velocity, another experiment was created, using high-speed cameras and the latest generation of high-power LEDs to obtain enough light within the short pulse widths required at high flow velocities.

The experiment was set up in the same cylindrical chamber, in which the convection experiment was conducted (see paragraph 2.1). An air jet generated by a fan (PHYWE - 02742-93, upper and lower screen removed) with a nozzle exit diameter of $D = 11\text{cm}$ and a variable exit velocity hits a flat acrylic glass plate at a distance of $H = 55\text{cm}$, $H/D = 5$, and at an angle of $\theta = 90°$. In the large measurement volume adjacent to the wall ($450\times500\times150\text{mm}^3$) the flow is seeded with helium-filled soap bubbles (HFSB) with diameters ranging from of $\sim 300\mu\text{m}$ to $\sim 500\mu\text{m}$, depending on the air pressure applied on the generator (LaVision HFSB generator). Six high-speed cameras (PCO dimax) record particle images at different frame rates, ranging from $f = 1.25\text{kHz}$ to $f = 3.9\text{kHz}$, depending on the flow velocity.

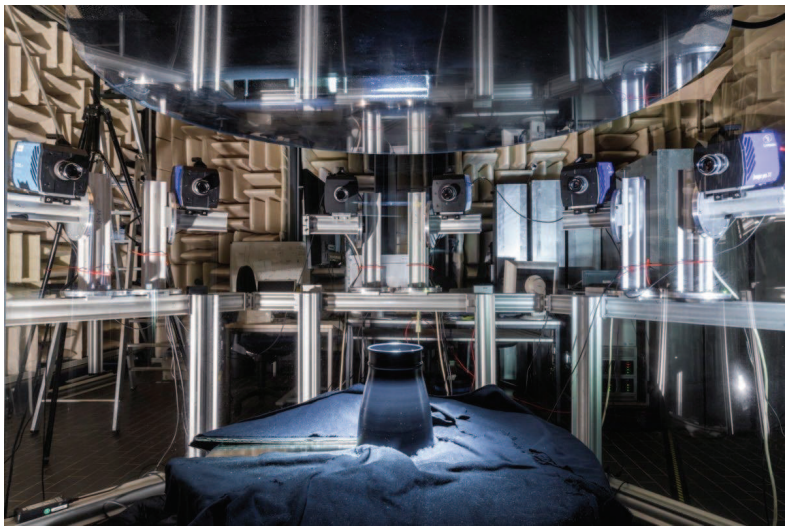

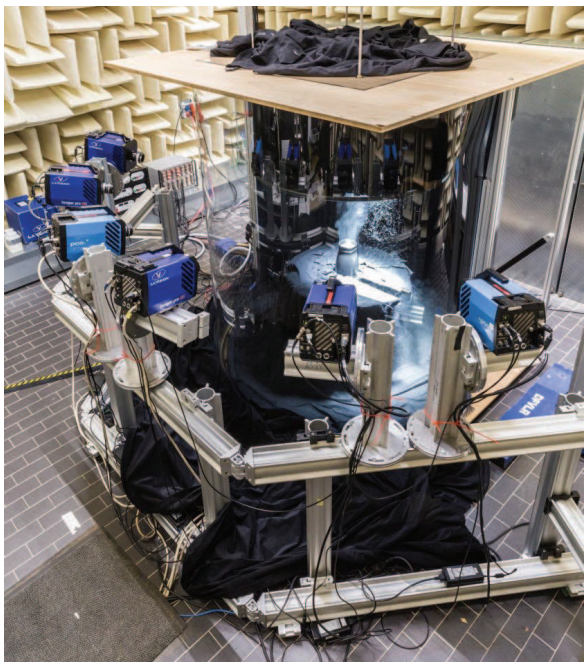

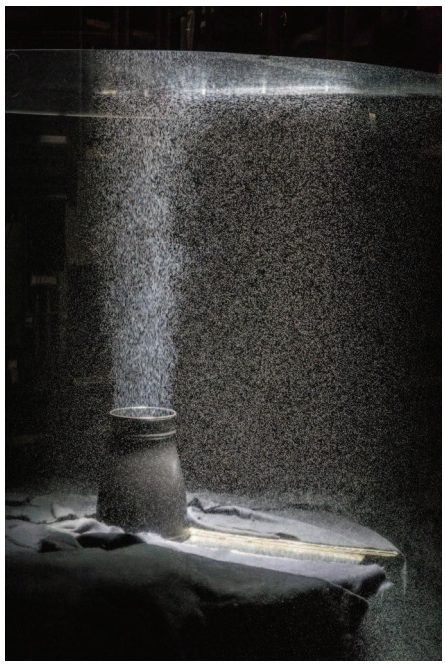

Figure 13: Photographs of the impinging jet experiement. Top: nozzle as viewed by the cameras sytem; down left: overview of the experimental apparatus; down right: nozzle in operation, emitting a turbulent jet, which impinges on the acrylic plate 55 cm above. The illuminated region can be recognized, with the light exiting through a passe-partout above the acrylic plate and being backreflected by a mirror below the nozzle.

The cameras are positioned in an in-line configuration and oriented in a way that lines of sight are tangential to the flat plate. The HFSBs are illuminated by two different pulsed LED arrays from above (through the acrylic glass plate). The central jet core is illuminated by a circular array of 150 high power LEDs, operated at 20 A (LaVision prototype); a double HARDsoft array of 42 LEDs each (operated at 90 A) is illuminating an area of approx. 20 cm in depth and 45 cm in

radial direction along the glass plate. The LEDs are operated at 10 % duty cycle. See Figure 13 for images of the setup.

Flow measurements at different jet velocities and aquisition rates were realized. The acquisition rate has to be increased accordingly, in order to restrict the particle shifts to no more than approx. 20 pixels. The usable resolution of the cameras sinks with the acquisition frequency, therefore reducing the imaged volume. At full resolution (which is in this case usable up to jet exit velocities of approx. 5 m/s) a volume of 47 liters could be reconstructed. At the highest repetition rate (3.9 kHz) the volume decreases to around 13 liters.

In order to ensure sharp particle imaging - avoiding temporal streaking - the pulse width – and therefore the available light – has to be reduced accordingly. For the shortest pulse widths an increase of the bubble size from 300 μm to 500 μm can increase the amount of reflected light reaching the cameras.

Operating at 1.25 kHz, using the full camera resolution, large numbers of bubbles (up to 190,000) could be successfully tracked with reliability similar to what has been demonstrated in the thermal plume experiment. Decreasing the pulse width leads to decreased signal-to-noise ratio, however even at a pulse-width of 27 μs the image quality allows for a very reliable tracking at seeding densities up to 0.045 ppp. Probably, even higher particle image densities could be processed. However, at high jet velocities (> 10 m/s) it was not possible to generate more bubbles, as likely a large number was destroyed by the blades of the fan.

Three exemplary cases were chosen for presentation within this text. Table 1 summarizes the main parameters of these cases. Very different jet velocities are presented, in order to document the differences in tracking properties, attainable volumes and resolvable scales.

Jet velocity [m/s]	Acquisition Rate [kHz]	Bubble size [μm]	Pulse width [μs]	Image size [px]	Volume [mm³]	Number of inst. tracked bubbles
1	1.25	~300	80	2016×2016	450×530×200	106,000
5.5	2	~500	50	1344×1808	370×530×200	118,000
16	3.9	~500	27	576×1728	180×530×140	40,000

Table 1: Parameters for volumetric measurements on impinging jet for different flow velocities

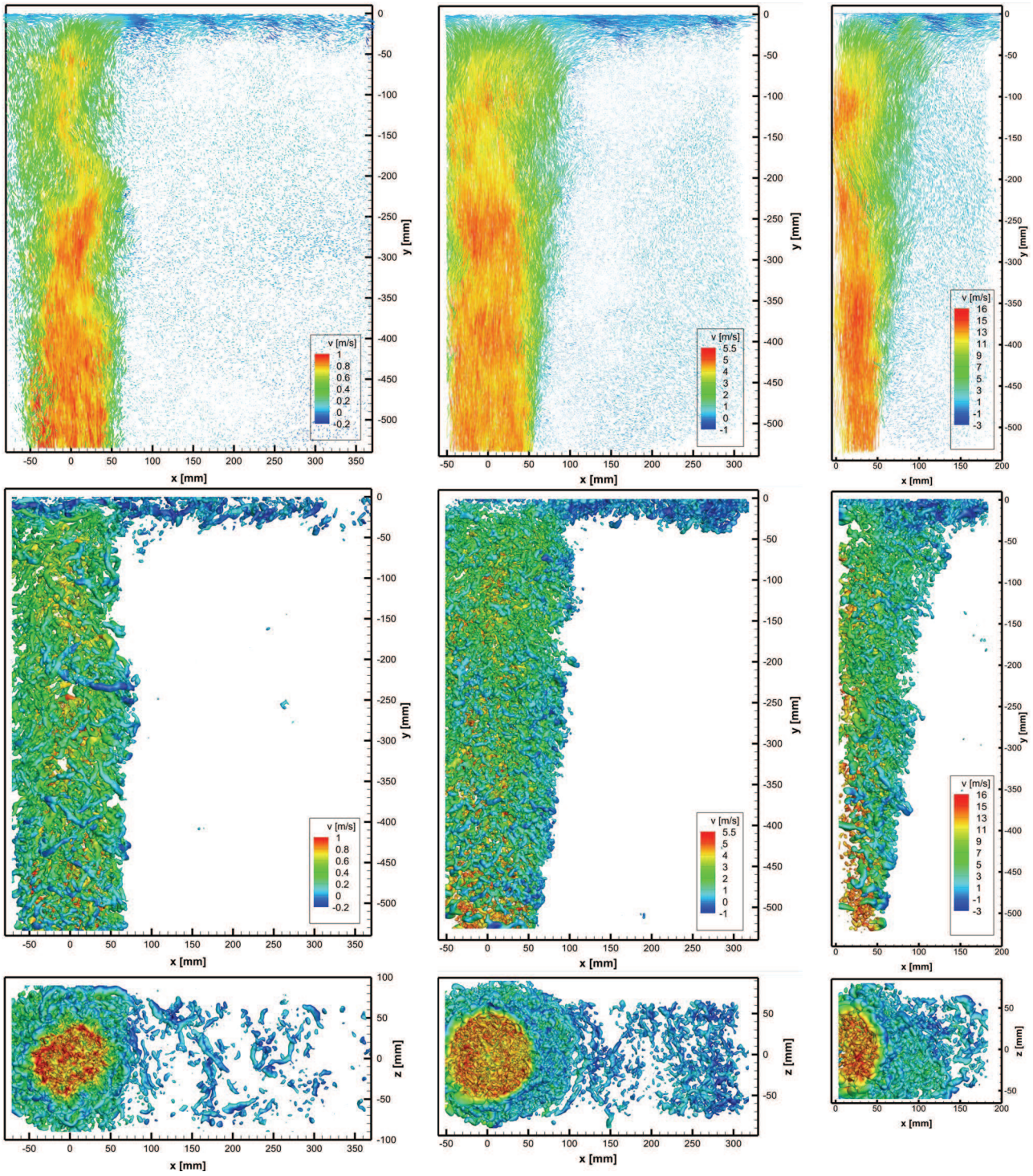

Figure 14: Results from STB + FlowFit evaluations for three flow velocities (from left to right 1 m/s, 5.5 m/s, 16 m/s) of an impinging jet. The top row shows velocity vectors of 9 successive time-steps from a 60 mm-slice in the center of the volume, color-coded by streamwise velocity. The second row displays isosurface of the Q-criterion, as extracted from FlowFit (from left to right: $Q = 700/s^2$; $Q = 25{,}000/s^2$; $Q = 150{,}000/s^2$) for the middle time-step. The third row shows the same isocontours, albeit looking upwards towards the impinging plate.

The following STB parameters were applied to all datasets: The number of triangulation iterations was set to 1, followed by one triangulation iteration using a reduced set of cameras. Each of these was followed by five shake-iterations (n_1= 1, n_2=1, m = 5, ε = 1.0; see (Wieneke 2013)). The allowed triangulation error was set to 1.0 pixel. For the initialization phase (the first four images), the number of triangulations was doubled. The search radius for new tracks was chosen according to the expected particle shift. As soon as enough tracks are present to serve as predictor for the track identification, a constant search radius of 4 pixels around the predictor point was used. Outliers were identified using a neighborhood criterion (velocity difference larger than 8 times the rms). All cases quickly converged to a stable solution; from there on, the algorithm can quickly work through the time-series, as only few particles need to be newly triangulated (typically 1,000-3,000). As a reference, for the 3.9 KHz-case 2,500 images could be processed with two passes of STB overnight on a 20-core server.

Following a successful tracking of the particles, FlowFit (Gesemann et al. 2016) was applied to the results. In contrast to the thermal plume case, which is driven by density gradients, the full Navier-Stokes regularization of FlowFit (including the material derivative) can be used in this case. A closely spaced system of Cubic B-splines is setup (here around 0.04 particles per cell); the resulting equation system is iteratively solved using an LBFGS solver. The gained continuous function is closely sampled on a grid with 1 mm spacing, resulting in velocity volumes of 540 points in streamwise direction and varying width and depth, depending on the case.

Figure 14 shows examplary snapshots from the tracked particles and the FlowFit results from two perspectives. It can be seen that for all cases the tracking system was able to extract bubble trajectories at high numbers. Visual inspection shows no traces of obviously falsely tracked particles. Turning to the FlowFit results, for the lowest velocity (1 m/s, Figure 14 left) a multitude of flow structures can be identified using the Q-criterion. The flow coming form the fan is in a turbulent state, however large, elongated vortices can still be detected. Especially along the impinging plate well defined structures can be seen. At higher velocities (5.5 m/s, Figure 14 middle) the structures become smaller and higher in number (please note the increasing threhold value for the isosurfaces). While the larger structures can still be resolved – notably at the impinging plate – the small structures are most likely underresolved. When looking at a time series (not available here) the small structures start to flicker between the different time-steps. At the highest velocities (16 m/s, Figure 14 left) the structures become even stronger (again, note the isosurface threshold), as the turbulence increases. Still, the FlowFit method is able to extract temporally coherent large structures from the STB tracks; the small scales are not fully resolved in this highly turbulent dataset.

While the interpolated result might not resolve all scales, the particle tracks still contain this information. Particle statistics (PDFs, Bin ensemble averaging) should be free of any bias, as long as the temporal resolution is high enough.
The volumetric results from the impinging jet measurements will also be used for volumetric pressure reconstruction. Three reference microphones were integrated into the impinging plate (see Huhn et al. 2016 for details)

6. Conclusions and Outlook

Large-scale time-resolved volumetric flow measurements on a thermal plume and on an impinging jet in air were presented. In both cases Helium filled soap bubbles are used as flow tracers and are illuminated by an array of high power white LEDs.
The thermal plume investigation used a measurement volume of 550 liters. Up to 275.000 bubbles could be tracked simultaneously using the Shake-The-Box algorithm. Highly resolved vector volumes of velocity and acceleration, interpolated onto an Eulerian grid using the FlowFit method, show multitudes of flow structures. To the knowledge of the authors this investigation contains both the largest volume in which instantaneous flow measurements were successfully performed as yet and the largest number of tracked particles for PTV experiments.
These features can be realized mainly due to the high image quality. The bubble size distribution is very sharp around 300 μm (monodisperse) and all bubbles scatter the light very similarly to all cameras. The white, uncoherent light produced by the LEDs avoids effects like speckles or interference, leading to temporally very consistent particle images. All these aspects are beneficial for a reliable tracking process of STB and allow for the high particle concentrations of up to 0.1 ppp.
In order to demonstrate the possibilities of performing similar measurements at much higher flow velocities, enabling the operation in typical wind tunnel experiments, a second experiment using high-speed imaging of the flow of an impinging jet was carried out
Brighter LEDs of the latest generation, were operated in the kHz-range, allowing the tracking of bubbles at flow speeds of up to 16 m/s. While the volume was smaller in this case (ranging from 13 to 47 liters, depending on the repetition rate), solutions to enlarge the usable volume are foreseeable. The high-power LED arrays used for this investiagtion are still under development and therfore the availablity was limited. In the future the illumination of larger volumes, using large arrays of LEDs can be attained. Combined with new generations of cameras, that allow higher frame-rates at higher resolutions, the volume size and usable flow speeds can be further

expanded into regimes that are typical for low-speed wind tunnel experiments (e.g. 60 m/s). Applying such a setup to a wind tunnel measurement requires a much higher number of bubbles (Scarano et al. 2015), compared to the closed cell used in these experiments. However, bubble generators with 50 or more nozzles are just becoming available, possibly solving this problem in the near future.

References

Biwole PH, Yan W, Zhang Y, Roux JJ (2009) A complete 3D particle tracking algorithm and its applications to the indoor airflow study. Meas Sci Technol 20 115403

Bosbach, J., Kühn, M., Wagner, C. (2009) Large scale particle image velocimetry with helium filled soap bubbles, Exp. Fluids 46, 539-547

Elsinga G E, Scarano F, Wieneke B and van Oudheusden BW (2006) Tomographic Particle Image Velocimetry. Exp Fluids 41:933–947

Gesemann S, Huhn F, Schanz D and Schröder A (2016) "From Noisy Particle Tracks to Velocity, Acceleration and Pressure Fields using B-splines and Penalties", 18th Int Symp on the Application of Laser Techniques to Fluid Mechanics, July 4-7, Lisbon, Portugal

Gilet T, Scheller T, Reyssat E, Vandewalle N, and Dorbolo S (2007) How long will a bubble be? arXiv:0709.4412

Huhn F, Schanz, Gesemann S, Schröder A (2016) FFT integration of instantaneous 3D pressure gradient fields from Lagrangian particle tracking in turbulent flows. 18th Int Symp on Applications of Laser Techniques to Fluid Mechanics, (Lisbon, Portugal, July 04-07)

Kähler CJ, Astarita T, Vlachos PP, Sakakibara J, Hain R, Discetti S, La Foy R, Cierpka C (2016), Main results of fourth International PIV Challenge, Exp. Fluids 57:97, DOI: 10.1007/s00348-016-2173-1

Klimas P (1973) Helium bubble survey on an opening parachute flow field. J Aircraft 10:567-569

Kühn, M., Ehrenfried, K., Bosbach, J., and Wagner, C. (2011) Large-scale tomographic particle image velocimetry using helium-filled soap bubbles, Exp. Fluids 50, 929-948

Maas, H G, Grün A, Papantoniou D (1993) Particle Tracking in three dimensional turbulent flows – Part I: Photogrammetric determination of particle coordinates. Exp Fluids 15:133-146

Malik N, Dracos T, Papantoniou D (1993) Particle Tracking in three dimensional turbulent flows – Part II: Particle tracking. Exp Fluids 15:279-294

Melling A (1997) Tracer particles and seeding for particle image velocimetry. Meas. Sci Technol 8:1406

Müller RHG, Flögel H, Schere T, Schaumann O, Markwart M (2000) Investigation of large scale low speed air conditioning flow using PIV. 9th Int Symp on Flow Visualization, Edinburgh, UK

Pounder E (1956) Parachute inflation process Wind-Tunnel Study, WADC Technical report 56-391, Equipment Laboratory, Wright Patterson Air Force Base. Ohio, USA, pp 17-18

Scarano, F., Ghaemi, S., Caridi, G., Bosbach, J., Dierksheide, U., Sciacchitano, A: On the use of helium-filled soap bubbles for large-scale tomographic PIV wind tunnel experiments, Exp. Fluids, 311 56:42, 2015.

Schanz D, Gesemann S, Schröder A (2016) Shake-the-box: Lagrangian particle tracking at high particle image densities. Exp Fluids 57:70

Schanz D, Gesemann S, Schröder A, Wieneke B, Novara M (2013a) Non-uniform optical transfer functions in particle imaging: calibration and application to tomographic reconstruction. Meas Sci Technol 24 024009

Schanz D, Schröder A, Gesemann S, Michaelis D, Wieneke B (2013b) Shake-the-Box: a highly efficient and accurate Tomographic Particle Tracking Velocimetry (TOMO-PTV) method using prediction of particle position. 10th Int. Symposium on Particle Image Velocimetry – PIV13 (Delft, The Netherlands, July 1-3)

Schneiders JFG, Azijli I, Scarano F, Dwight RP (2015) Pouring time into space. 11th Int. Symposium on Particle Image Velocimetry – PIV15 (Santa Barbara, California, September 14-16)

Tobin, S.T., Meagher, A.J., Bulfin, B., Möbius, M., Hutzler, S.: (2011) A public study of the lifetime distribution of soap films, Am. J. Phys. 79(819), 819-824

Wieneke B (2013) Iterative reconstruction of volumetric particle distribution. Meas. Sci. Technol. 24:024008